PHYSICAL REVIEW FLUIDS **7**, 043702 (2022)

Controlling instabilities of electrified liquid jets via orthogonal perturbations

Chenghao Xu, Wuqing He, Weiwei Yang, Weiwei Deng, and Huihui Xia[*]
Department of Mechanics and Aerospace Engineering, Southern University of Science and Technology, Shenzhen 518055, China

(Received 12 August 2021; accepted 4 April 2022; published 15 April 2022)

Whipping is a peculiar nonaxisymmetric instability experienced by electrified liquid jets and utilized in electrospinning to produce fine polymer fibers; however, it manifests itself in a chaotic and uncontrollable fashion. We impose two perturbations in the form of small mechanical oscillations, orthogonal with each other, to alter and curb instabilities of electrified liquid jets. The oscillations cause transverse positioning disturbance to the nozzle and therefore the initial positioning of the jet. The effects of parameters including the excitation frequency, amplitude, and phase difference of the imposed perturbations and the axial electric field are investigated. The steady helicoidal whipping structure with a linearly growing lateral amplitude in air has been demonstrated, offering a feasible solution for electrospinning to fabricate fibers of uniform thickness. Furthermore, the superposition of two sinusoidal orthogonal perturbations enables deposition of complex patterns, such as Lissajous curves.

DOI: 10.1103/PhysRevFluids.7.043702

I. INTRODUCTION

The presence of an intense electric field may introduce instabilities to liquid jets distinct from those observed with their electrically neutral counterparts owing to the Coulombic repulsion resulting from induced net charges at the jet interface [1–4]. One of these distinctive instability phenomena is known as the whipping or kink mode, manifesting itself as rapid lateral motion and lashes. The resultant large tensile stresses empower the utility of this mode in the production of ultrathin fibers [5,6]. This is the fundamental mechanism exploited in electrospinning, where polymer fibers down to nanometers in diameter are produced [7]. Such fibers of remarkably high aspect ratios make electrospinning competitive in applications such as nanotechnology and life science [8–10].

Once an electrified jet moves off its original axis, the nonaxisymmetric electrostatic repulsion will push the curved portion further away; as a result whipping instabilities are formed. Unfortunately, the dynamics of electrified jets is subject to random perturbations in most experimental practices and manifests in a chaotic fashion [11]. This undesirable feature brings forth challenges in keeping the ordered whipping structure of electrospinning and undermines the quality of the produced fibers. To overcome this problem, materials scientists usually resort to methodologies such as shortening the electrospinning distance [12] and optimizing the moving speed of substrates to suppress irregular depositions [13]. Fluid dynamicists are also interested in the electrified whipping jet, especially the formation mechanism and properties of whipping structures [14]. Several publications report achieving steady helicoidal structures of whipping in liquid ambience, taking advantage of the fact that the characteristic time of jets is much longer than that in air [15–17]. Very few works have been conducted in air, with the exception of Yang *et al.* [18], who utilized alternative

---

[*] xiahh@sustech.edu.cn

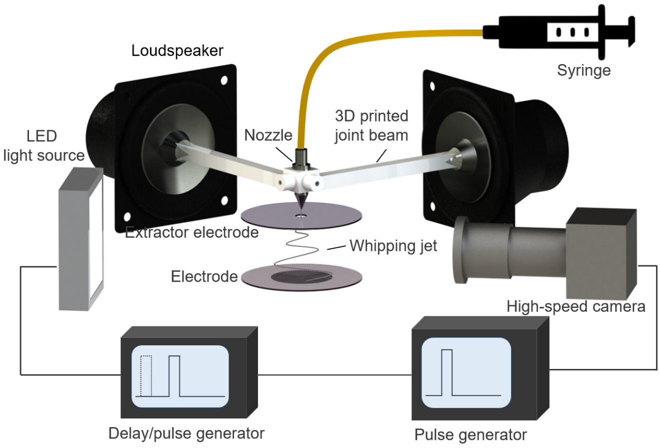

FIG. 1. Schematic of experimental device for controlling instabilities of electrified jets via orthogonal perturbations imposed by two loudspeakers.

electric fields to generate in-plane transverse perturbations that realized the transition from varicose to whipping instabilities in air. However, the jet motion in their experiments was confined in the planar space and achieving controllable whipping structures in a general manner remains an open issue.

Since jet instabilities originate from the evolution of perturbations, it is possible to curb the dynamics of electrified jets by imposing specific forms of perturbations. Indeed, in the prevailing numerical model developed by Reneker and co-workers for electrospinning [19,20], orthogonal perturbations of identical frequency and amplitude are prescribed at the spinneret exit. Based on simulations using this model, Coluzza *et al.* reported that increasing the amplitude and frequency of the driving perturbations could expand the opening angle of the spiral structures and reduce the jet thickness in electrospinning [21,22]. In this work, we designed a device to introduce orthogonal perturbations transverse to the electrified jets in air ambience, and we investigated the effects of parameters, including the frequency, amplitude phase difference, and axial electric field strength in steady helicoidal whipping structure. In addition to the helicoidal structure, interestingly, with further varying of the frequency and phase difference, we found more distinct jet instability modes corresponding to the initial perturbations.

II. EXPERIMENTAL METHODS

We used two loudspeakers with their cone centers bonded to a three-dimensional (3D)-printed right-angle joint beam to allow the superposition of two orthogonal mechanical oscillations, as shown in Fig. 1. A stainless-steel nozzle was embedded at the beam joint so that transverse perturbations of the initial positioning of the jet are introduced. The loudspeakers were driven by sinusoidal input voltages, respectively defined as

$$\begin{aligned} s_1(t) &= A\sin(2\pi f_1 t), \\ s_2(t) &= A\sin(2\pi f_2 t + \phi), \end{aligned} \tag{1}$$

with A, f, and ϕ being the amplitude, frequency, and phase difference. In this manner, the perturbation pattern of the jet initial position follows the superposition of the sinusoidal vibrations. For instance, when $f_1 = f_2$ and $\phi = \pm\pi/2$, the superposed pattern of orthogonal perturbations is a circle. Perturbations in the circular pattern enable whipping in a helicoidal structure [21], which is fundamental to producing controllable uniform fibers. Note that the vibration amplitude at various driving voltages and frequencies needs to be calibrated (see Supplemental Material [23]).

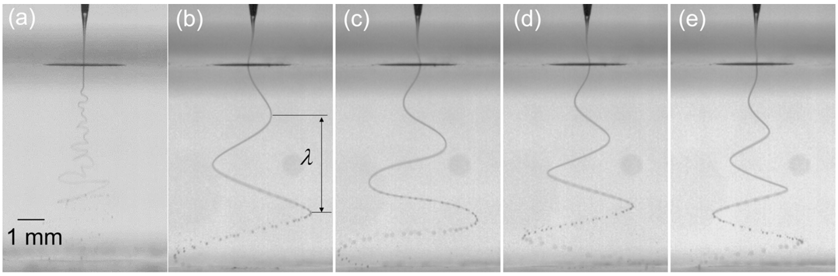

No imposed perturbations

$f_1 = f_2 = 1.4$ kHz
$\lambda = 3.5$ mm

1.8 kHz
2.7 mm

2.0 kHz
2.5 mm

2.4 kHz
2.1 mm

FIG. 2. Examples of (a) chaotic whipping with no imposed perturbations and (b–e) helicoidal whipping structures of jets emanated from the Taylor cone at constant flow rate $Q = 300\,\mu l/\text{min}$ and axial electric field strength between the two parallel electrodes $E_z = 6$ kV/m .

We used triethylene glycol (TEG), an organic liquid of mediate viscosity $\mu = 49$ mPas, surface tension $\gamma = 45.3$ mN/m, and electric conductivity $K = 1.8 \times 10^{-5}$ S/m. The liquid jet was issued from the nozzle (inner radius $R_{\text{in}} = 120\ \mu$m and outer radius $R_{\text{out}} = 180\ \mu$m) at a constant flow rate delivered by a syringe pump. To charge the jet, a constant high negative voltage was applied on a round extractor electrode mounted 3 mm below the nozzle tip. A second meshed electrode applied with a lower negative voltage was mounted parallelly below the extractor electrode, establishing a nearly uniform axial electric field E_z. We visualized the jet with a high-speed camera (i-SPEED 220, iX Cameras) with a long-distance lens of adjustable magnification in shadowgraph mode at 2852 frames per second with an exposure time of 10 μs. The region of interest was illuminated from behind with a large-area (9×9 cm^2) light emitting diode (LED) light source (OPT-FLP9090-W, OPT). The current I was obtained by measuring the voltage drop V_m through a multimeter (Fluke 12E+ Digital Multimeter), which is connected in series with the nozzle and has an internal resistance of 10 MΩ.

III. RESULTS AND DISCUSSIONS

A. Steady helicoidal whipping structure in the cone-jet mode

We use the Weber number $\text{We} = \rho Q^2/(\pi^2 \gamma R_{\text{in}}^3)$ to assess the relative importance of inertia and surface tension, where ρ is the liquid density. When the flow rate Q is too low, the Weber number is less than unity, and the flow takes the form of dripping instead of jetting. An intense electric field between the nozzle and extractor can accelerate the liquid to form a Taylor cone with a fine jet erupting from the apex of the cone, which is known as the cone-jet mode. With the aid of orthogonal perturbations of identical frequency and phase difference equal to $\pi/2$, and if the imposed perturbations grow fast enough, a helicoidal whipping structure is formed downstream [21]. Figure 2 demonstrates a chaotically whipping jet without imposing perturbations and steady 3D helicoidal morphology of the whipping jet in the cone-jet mode at various excitation frequencies (see Supplemental Material [23]). The liquid feeding flow rate was $Q = 300\,\mu$l/min, and We ≈ 0.3 within the nozzle. We observed that the number of turns of the jet between the two parallel electrodes increases linearly with the excitation frequency, as defined in the axial wave number $\chi = 2\pi R/\lambda$ with R representing the jet radius, and λ the wavelength. This indicates that the morphology of the spiral depends highly on the initial perturbations. The steady helicoidal whipping structure is characterized with a constant envelope angle and a linearly growing lateral amplitude, in line with previous results obtained in the liquid ambience [16]. The axial component of the whipping velocity, namely, the phase velocity, is calculated by $u_z = \lambda f \approx 5.0$ m/s. Accordingly, the averaged local Weber number at the corresponding whipping segment is larger than 10. This value is one order of magnitude higher than that at the nozzle and consistent with the stability condition for jetting. Moreover, compared with the experiments of Yang *et al.* where ethanol was used [18], varicose instabilities are substantially suppressed as TEG's viscosity is over 40 times higher and as a result, the jet exhibits more turns before breaking up. More importantly, the jet thickness reduces smoothly downstream before the varicose instability dominates with the ordered helicoidal structure. This outperforms chaotic whippings and in-plane whippings induced from one-dimensional perturbations [18], as fibers of uniform thickness can be produced.

B. Effects of the excitation frequency

Given that the amplitude of the imposed perturbations stands out from the background noise, the breakup process of the jet is highly repetitive and controllable. Here, we focus on the condition that the two speakers have equal excitation frequency and constant phase difference (90°) as demonstrated in the previous section. We can gain deeper insights into the controlling of electrified jet instabilities from simplified linear stability theory without considering nonlinear effects. We rewrite Saville's equation describing the dispersion relationship for electrified Newtonian viscous liquid cylinders [24]:

$$1-\chi^2-m^2-\Gamma\left[1+\chi\frac{K'_m(\chi)}{K_m(\chi)}\right]=2\mathrm{Oh}\chi^2\omega\frac{\det D_1}{\det D_2}, \tag{2}$$

where $\omega=\hat{\omega}\sqrt{\rho R^3\gamma}$ is the normalized growth rate with $\hat{\omega}$ defined as the growth rate; K_m denotes the modified Bessel function of the second kind; m is the azimuthal wave number, with $m=0$ denoting the varicose mode and $m=1$ the sinusoidal (whipping) mode. The dimensionless numbers Γ and Oh are the electrical Bond number and the Ohnesorge number, respectively defined as $\Gamma=\sigma^2R/(\gamma\varepsilon_0)$ and $\mathrm{Oh}=\mu/\sqrt{\gamma\rho R}$ with ε_0 being the permittivity of free space, and σ the surface charge density obtained from the convection current $\sigma=I_{\mathrm{conv}}R/(2Q)$. The last term on the right-hand side refers to the ratio between determinants of D_1 and D_2, where the details can be found in Eqs. (11) and (12) in Saville's paper [24]. According to the dispersion relationship, the transition frequency from the whipping to the varicose mode could be up to hundreds of kilohertz, since the diameter of a jet emanated from the Taylor cone typically falls within the order of 10 μm. Here, we increase Q to 5.5 ml/min (same as below unless otherwise specified) to shift the jetting from the cone-jet to the simple-jet mode [25,26]. In this case the Weber number at the nozzle exit equals 10, surpassing the threshold condition ($\mathrm{We}>4$) for issuing an electrically neutral jet [27]. By this means, the jet radius is equal to the inner radius of the nozzle, and the transition frequency decreases to kilohertz, just within the operating regime of the loudspeakers. It is worth mentioning that the conduction current $I_{\mathrm{cond}}=\pi R^2KE_z$ cannot be neglected here as the jet is one order of magnitude thicker than typical jets in cone-jet mode. In our experiments, I_{cond} reached the order of 100 nA, which can be half of the total measured current. Henc, we have $I_{\mathrm{conv}}=I-\pi R^2KE_z$.

Figure 3 shows the typical images capturing the transition from the whipping to the varicose mode by continuously increasing the excitation frequency (see Supplemental Material [23]), and the dispersion relations based on Eq. (2) when $\Gamma=1$, and $\mathrm{Oh}=0.6$. At low excitation frequency [Fig. 3(a)], the jet manifests a helicoidal structure, as the growth rate of the whipping instability is larger than that of the varicose instability. The maximum whipping growth rate occurs at around 0.75 kHz [see Fig. 3(h)]. With increased excitation frequency, the breaking-up point gradually moves upstream, as the varicose mode becomes increasingly prominent. Further increasing the excitation frequency, the increase in the varicose growth rate leads to earlier breakup [Fig. 3(b)]. Above some frequency (∼1.4 kHz), the varicose instability grows faster than the whipping. When the second harmonic of the excitation frequency reaches the Rayleigh frequency (∼1.6 kHz), while the whipping instability also plays a role [not exactly captured in Fig. 3(h)], the helicoidal structure collapses into fractured filaments and two streams of monodispersed droplets [Figs. 3(c) and 3(d)]. This phenomenon is similar to the whipping assisted bifurcation mode reported in the experiments of Yang *et al.* [18]. It is found that the bifurcation streams rotate synchronously when varying

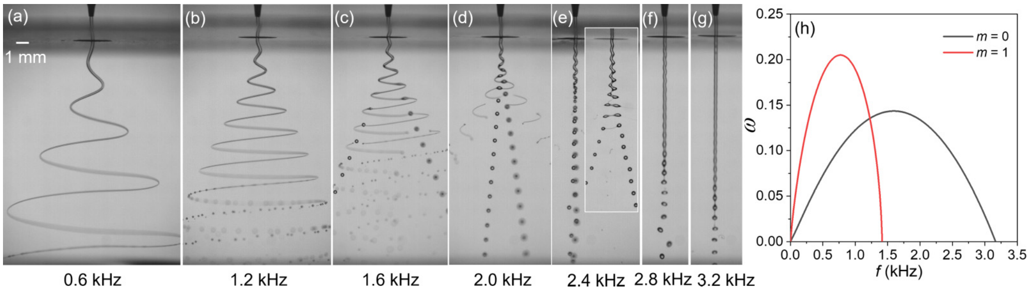

FIG. 3. [(a)–(g)] Example images of instability transition of electrified jets via changing the excitation frequency of orthogonal perturbations, and (h) the corresponding dispersion curves based on Eq. (2). The inset of (e) is its side view. The axial electric field $E_z = 1.15 \times 10^5$ V/m.

excitation frequency, indicating that their phases are not constant. This evidence rules out the possibility that any imperfection of imposed perturbations plays a major role in the formation of bifurcation. Different from Yang's observations, filaments cut off by the two main droplets are formed due to significant viscous effects and eventually break into much finer droplets. At higher excitation frequency, due to the zero growth rate of whipping, the filaments are not seen, and instead, dumbbell-shaped segments are yielded [Fig. 3(e)]. Although a sinusoidal wave is visible at 2.8 kHz, it gives way to the varicose instability downstream. Above 2.8 kHz, the jet is straight as governed by the varicose instability. Since the varicose growth rate declines, the jet is elongated when increasing the excitation frequency.

At large wave numbers, the growth rate associated to the varicose breakup is larger than that of the whipping instability, while this trend is reversed for small wave numbers. It is noted that when increasing the excitation frequency, the measured current did not remain constant, with its value declining in the whipping mode and increasing in the varicose mode. Therefore, the value of Γ also varied, as shown correspondingly in Fig. 4. The jet instabilities are mapped in the χ-Γ diagram,

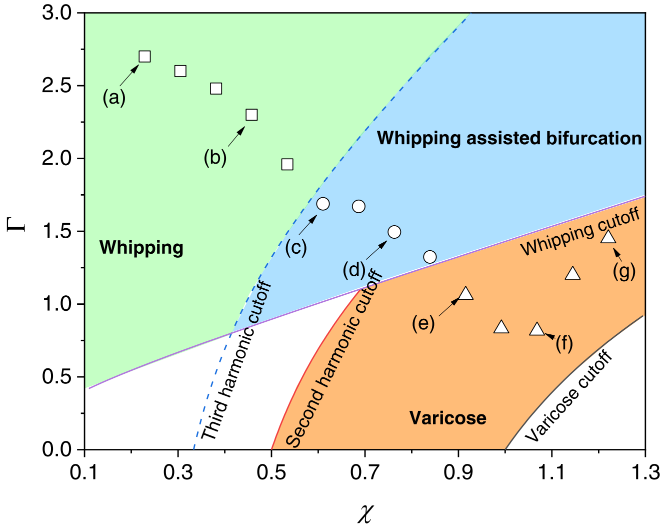

FIG. 4. Jet instability mode mapped in the χ-Γ diagram, where the whipping mode is denoted by the green background, whipping assisted bifurcation mode is the region in blue, and the varicose mode is in orange. The data points are the corresponding experimental data partially marked in Fig. 3.

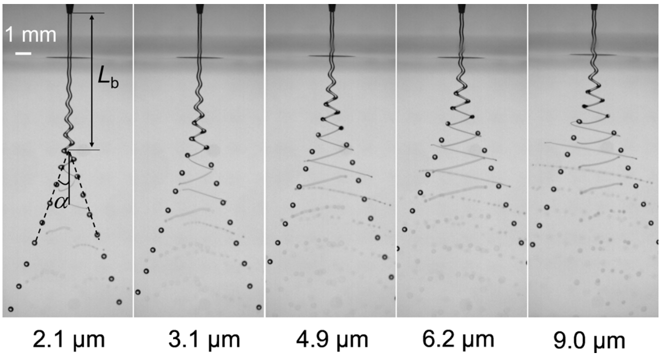

FIG. 5. Snapshots of the whipping assisted bifurcation mode at various initial perturbation amplitudes at constant excitation frequency of 1.8 kHz.

partitioned by cutoff curves obtained Eq. (2). The cutoff curves refer to the zero growth rate of specific instability, below which the corresponding instability vanishes.

C. Effects of the initial perturbation amplitude

As aforementioned in introducing our experimental setup, the amplitude of the initial perturbation A imposed by the loudspeakers varies with excitation frequency. Therefore, it is important to examine the influence of the initial perturbation amplitude, especially on the jet instability mode, although it should be trivial according to the dispersion relationship. We verify this by varying the driving voltage of the loudspeakers while keeping the excitation frequency constant at 1.8 kHz, specifically in the whipping assisted bifurcation mode, as illustrated in Fig. 5. When the amplitude of initial perturbations increases nearly four times from ~2 to 9 μm, the jet remains in such transition mode without either shifting to the varicose or the whipping mode. Hence, it is acceptable to only consider the role of the excitation frequency in the transition of instabilities as demonstrated in Fig. 3. On the other hand, it is noted that the bifurcating inception point moves close to the nozzle, when the initial perturbation amplitude is increased. This distance marked by L_b is plotted versus A in Fig. 6(a). The fitting shows that L_b approximately declines with A in a logarithm trend. This result is in agreement with the study of González and García on the jet length in the varicose mode, where an axial electric perturbation was adopted [28]. In addition, Fig. 6(b) shows the dependence of the semiopening angle α on the perturbation amplitude in the transition mode and the whipping mode ($f = 2.1$ kHz, $Q = 1.5$ ml/min). In the helicoidal whipping mode, there is significant growth of α when increasing A from 1 to 5 μm. Because larger amplitude causes larger displacement off the jet's axis, according to Earnshaw's theorem, the surface charge distributed along the jet will push this portion further away from its axis, resulting in a larger opening angle. This provides a clue that a higher initial perturbation amplitude promotes the production of thinner jets, due to the larger shearing force at a higher opening angle. On the other hand, α increases marginally with A in the whipping assisted bifurcation mode. An interpretation for this is that a larger perturbation amplitude leads to faster growth of varicose instability and earlier jet breakup, leaving shorter developing time for the off-axis instability. Besides, with relatively low surface charge density (Fig. 4), the opening angle is less sensitive to the initial perturbation amplitude. Nonetheless, the opening angle in both modes attempts to reach a plateau by only enhancing the perturbation amplitude, due to the increasing energy consumption by the counteracting factors, such as the viscous shearing (dissipation), capillary effect, and air drag. It can be explained why this observation is different from the numerical simulations in [21], where a linear relationship was drawn without considering the above factors.

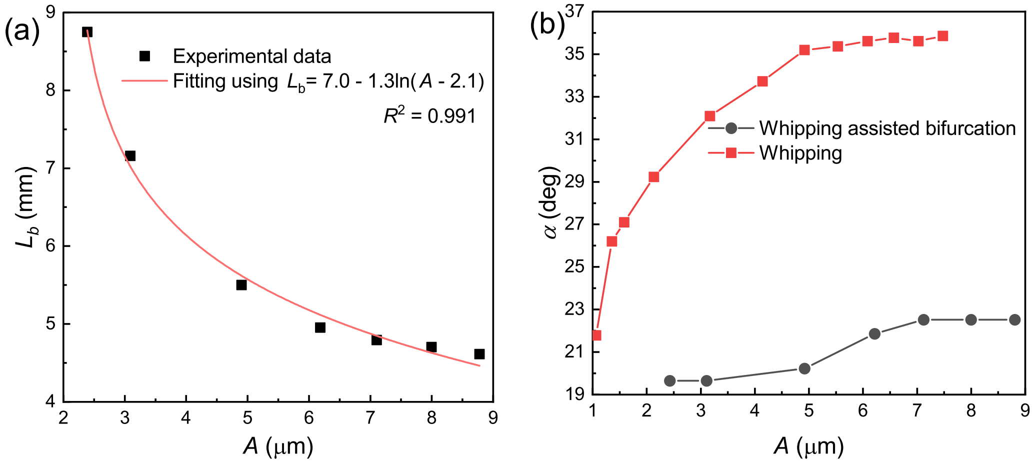

FIG. 6. Effects of the initial perturbation amplitude A on (a) the distance between the nozzle and the bifurcating point shown in Fig. 5, and (b) the semiopening angle in the whipping assisted bifurcation mode and the whipping mode

D. Effects of the axial electric field strength

We also explore effects of the axial electric field strength E_z by tuning the applied voltage on the lower electrode at a constant excitation frequency of 1.0 kHz. As shown in Fig. 7, the response of the helicoidal whipping jet to E_z is in analogy with applying a pulling or pressing force on a spring. Enhancing E_z elongates the wavelength and reduces the opening angle of the helicoidal structure in a linear manner, as quantitatively plotted in Fig. 8. In addition, the measured overall current increases approximately linearly with E_z, contributed by the increased conduction current $I_{\mathrm{cond}} = \pi R^2 K E_z$. One can estimate that the average jet radius is in the magnitude of a dozen microns from the fitting coefficient, in line with observations in Fig. 7. Moreover, with increased E_z, the jet is elongated in the axial direction and the growth of varicose instabilities is suppressed due to larger shearing force exerted on the jet This effect is also indicated by the local Weber number, as it rises from 6.6 to 19.1 with E_z, showing an increased importance of the inertial effect compared with the capillary effect. It can be concluded that the axial electric field strength can serve as an extra parameter for controlling the whipping structure and the resulting fiber thickness in applications of electrospinning.

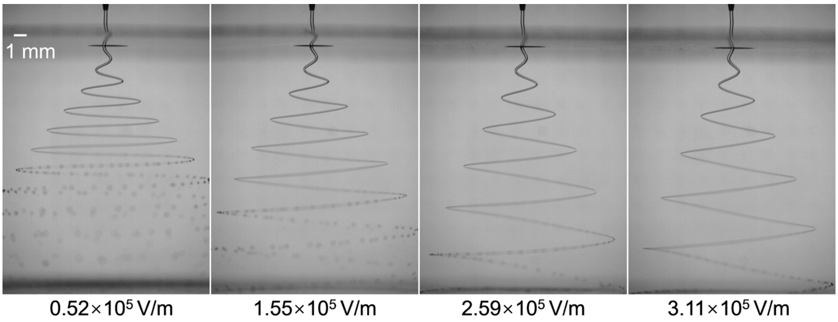

FIG. 7. Images of the helicoidal whipping structure obtained at various axial electric field strengths without changing other operating parameters.

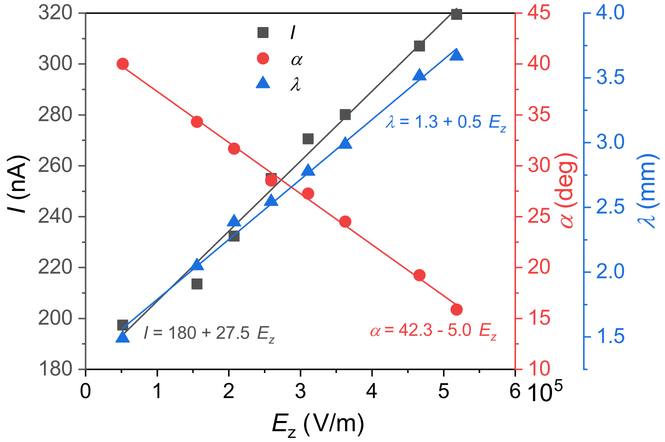

FIG. 8. Effects of the axial electric field strength on the overall current, half-cone angle, and averaged wavelength of the whipping structure.

E. Effects of the phase difference

We have demonstrated the functionality of the excitation frequency and amplitude of the orthogonal perturbations in controlling instabilities of electrified jets, while setting the superposed pattern of perturbations as a circle. Indeed, Eq. (1) describes a family of smooth curves known as Lissajous curves, having interesting properties and applications [29,30]. We can expediently differ the parameters of the orthogonal perturbations, taking advantage of the flexibility in controlling initial perturbations. Following the motivation of our recent work [31] for applications of film deposition using electrospray, we can gradually transform the superposition of the orthogonal perturbations from a circle into a line by simply adjusting the phase difference ϕ from $\pi/2$ to zero and accordingly "compress" the deposition pattern on demand, as shown by snapshots from two viewing angles in Fig. 9. Noticeably, as the whipping structure is compressed in one direction and slightly stretched in the other, the spiral turns to become a saddle-shaped profile with the stretched sides being "lifted" up, where the jet segments in fact move slower than other parts. This leads to oscillations of the shear stress along the jet and, as a result, the thickness of the jet segments in the vicinity of the turning point increases (see in view 1). Such phenomenology is exaggerated when further increasing the excitation frequency, as shown in Fig. 10, where the thick segments evolve and eventually break up into two streams of droplets, that is, the whipping assisted bifurcation mode. Moreover, it is found that with lower ϕ, the threshold of the excitation frequency for the inception

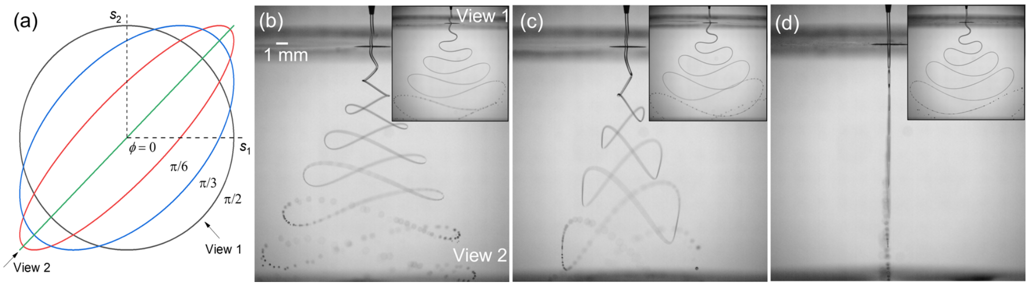

FIG. 9. (a) Patterns of orthogonal perturbation superposition at various phase differences, where the dashed lines s_1 and s_2 represent the imposed perturbation directions; [(b)–(d)] snapshots obtained from view 1 (insets) and view 2, when $\phi = \pi/3$, $\pi/6$, 0, respectively.

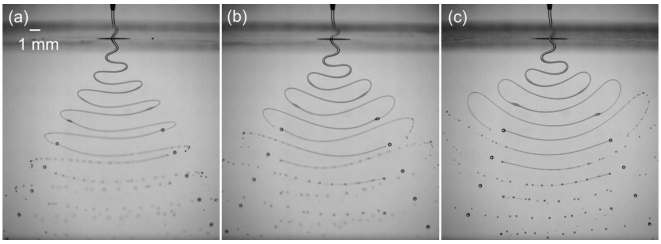

FIG. 10. (a) Snapshots obtained at the inception of whipping assisted bifurcation mode from view 1 at (a) $\phi = \pi/3$, $f = 1.0$ kHz; (b) $\phi = \pi/6$, $f = 0.95$ kHz; (c) $\phi = 0$, $f = 0.9$ kHz.

of the whipping assisted bifurcation mode decreases. Although the spikes of jet thickness along the axial direction are not desirable in electrospinning for fiber production, the compressed topology, especially when $\phi = 0$, demonstrates the potential in film deposition applications as long as the jet breakup into droplets is well handled.

F. Lissajous curves

As shown in Fig. 11, we further differ the phase difference ϕ and the excitation frequency f_1 and f_2. A diversity of Lissajous trajectories corresponding to the input perturbations are deposited on the lower electrode. For example, when $f_2/f_1 = 0.5$ and $\phi = \pi/2$, a figure “8” is observed. This reinforces the evidence that the whipping structure is highly dependent on the choice of input perturbations and is controllable. The superposition of two orthogonal perturbations provides a variety of controllable depositions on substrates. However, it should be noted that as also found in Fig. 9, the jet thickness also oscillates, which is detrimental in electrospinning applications.

We note that utilization of lateral electric fields is also an effective approach to control the whipping morphology. A main advantage compared with using mechanical oscillations is that it supports a much higher excitation frequency (>10 kHz), which covers the response range of excitation frequency for fine jets in practical applications. Lauricella *et al.* numerically studied the jet morphology controlling mechanism with an external rotating electric field transverse to the jet [32]. They used hexagonally arranged capacitor plates connected to a three-phase power source

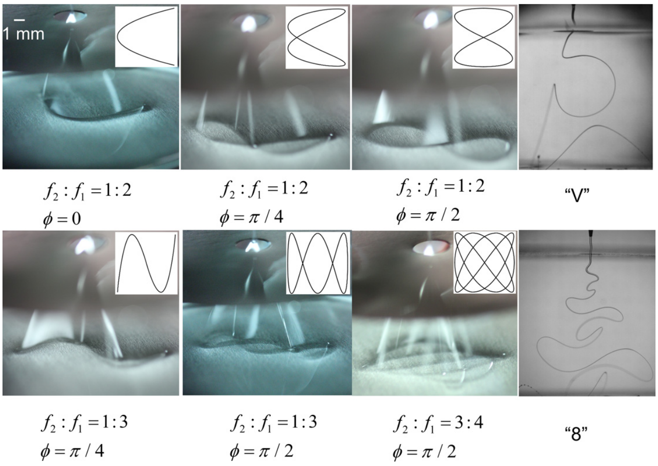

FIG. 11. Lissajous trajectories deposited on the lower electrode at various excitation frequency ratios and phase differences. The insets illustrate the corresponding imposed perturbation patterns. The high-speed images on the right show the jet morphology corresponding to figure “V” and figure “8”.

to reduce the resulting fiber thickness. It can be expected that by varying the electric field, the Lissajous trajectories are also achievable. However, it should be stressed that the electrodes need to be carefully designed and arranged to form a desired rotating electric field. For example, the electric field needs to "rotate" smoothly in terms of both space and time. This was not achieved in [32], as can be found from the jet morphology and deposition patterns on the substrate. Another problem in experimental practice is that the electric field between electrodes may be too high to cause spark. Future work can be conducted to improve this electrode configuration to controllably drive the fiber and its deposition.

IV. CONCLUSIONS

We have experimentally demonstrated that steady whipping structures described as a conical helix are achievable via imposing orthogonal perturbations to the electrified jet. The parameters, especially the frequency and phase difference, are critical in determining the jet instability mode. The approach of imposing periodic perturbations not only helps stabilize the whipping structure, but also offers an additional dimensional control in the production of electrified jets. The orthogonal perturbation enables superposition of fundamental sinusoidal signals of different frequency and phase to create complex Lissajous patterns, which show the unique ability of modulating the electrified jet in space via choreographed orthogonal perturbation.

ACKNOWLEDGMENTS

This work was financially supported by the National Natural Science Foundation of China (Grants No. 11802115 and No. 11932009) and GuangDong Basic and Applied Basic Research Foundation (Grant No. 2020A1515110268).

---

[1] J. Eggers and E. Villermaux, Physics of liquid jets, Rep. Prog. Phys. **71**, 036601 (2008).

[2] J. Rosell-Llompart, J. Grifoll, and I. G. Loscertales, Electrosprays in the cone-jet mode: From Taylor cone formation to spray development, J. Aerosol Sci. **125**, 2 (2018).

[3] H. H. Xia, A. Ismail, J. Yao, and J. P. W. Stark, Scaling Laws for Transition from Varicose to Whipping Instabilities in Electrohydrodynamic Jetting, Phys. Rev. Appl. **12**, 014031 (2019).

[4] J. M. Montanero and A. M. Gañán-Calvo, Dripping, jetting and tip streaming, Rep. Prog. Phys. **83**, 097001 (2020).

[5] M. M. Hohman, M. Shin, G. Rutledge, and M. P. Brenner, Electrospinning and electrically forced jets. II. Applications, Phys. Fluids **13**, 2221 (2001).

[6] J. Xue, T. Wu, Y. Dai, and Y. Xia, Electrospinning and electrospun nanofibers: Methods, materials, and applications, Chem. Rev. **119**, 5298 (2019).

[7] Y. M. Shin, M. M. Hohman, M. P. Brenner, and G. C. Rutledge, Electrospinning: A whipping fluid jet generates submicron polymer fibers, Appl. Phys. Lett. **78**, 1149 (2001).

[8] Z.-M. Huang, Y. Z. Zhang, M. Kotaki, and S. Ramakrishna, A review on polymer nanofibers by electrospinning and their applications in nanocomposites, Compos. Sci. Technol. **63**, 2223 (2003).

[9] Y. Dzenis, Spinning continuous fibers for nanotechnology, Science **304**, 1917 (2004).

[10] A. Luraghi, F. Peri, and L. Moroni, Electrospinning for drug delivery applications: A review, J. Controlled Release **334**, 463 (2021).

[11] T. Han, D. H. Reneker, and A. L. Yarin, Buckling of jets in electrospinning, Polymer **48**, 6064 (2007).

[12] D. Sun, C. Chang, S. Li, and L. Lin, Near-field electrospinning, Nano Lett. **6**, 839 (2006).

[13] D. Ye, Y. Ding, Y. Duan, J. Su, Z. Yin, and Y. A. Huang, Large-scale direct-writing of aligned nanofibers for flexible electronics, Small **14**, 1703521 (2018).

[14] M. Montinaro, V. Fasano, M. Moffa, A. Camposeo, L. Persano, M. Lauricella, S. Succi, and D. Pisignano, Sub-ms dynamics of the instability onset of electrospinning, Soft Matter **11**, 3424 (2015).

[15] G. Riboux, Á. G. Marín, I. G. Loscertales, and A. Barrero, Whipping instability characterization of an electrified visco-capillary jet, J. Fluid Mech. **671**, 226 (2011).

[16] J. Guerrero, J. Rivero, V. R. Gundabala, M. Perez-Saborid, and A. Fernandez-Nieves, Whipping of electrified liquid jets, Proc. Natl. Acad. Sci. U. S. A. **111**, 13763 (2014).

[17] C. Qi, Y. Li, Z. Liu, and T. Kong, Electrohydrodynamics of droplets and jets in multiphase microsystems, Soft Matter **16**, 8526 (2020).

[18] W. Yang, H. Duan, C. Li, and W. Deng, Crossover of Varicose and Whipping Instabilities in Electrified Microjets, Phys. Rev. Lett. **112**, 054501 (2014).

[19] D. H. Reneker, A. L. Yarin, H. Fong, and S. Koombhongse, Bending instability of electrically charged liquid jets of polymer solutions in electrospinning, J. Appl. Phys. **87**, 4531 (2000).

[20] A. L. Yarin, S. Koombhongse, and D. H. Reneker, Bending instability in electrospinning of nanofibers, J. Appl. Phys. **89**, 3018 (2001).

[21] I. Coluzza, D. Pisignano, D. Gentili, G. Pontrelli, and S. Succi, Ultrathin Fibers from Electrospinning Experiments under Driven Fast-Oscillating Perturbations, Phys. Rev. Appl. **2**, 054011 (2014).

[22] M. Lauricella, S. Succi, E. Zussman, D. Pisignano, and A. L. Yarin, Models of polymer solutions in electrified jets and solution blowing, Rev. Mod. Phys. **92**, 035004 (2020).

[23] See Supplemental Material at http://link.aps.org/supplemental/10.1103/PhysRevFluids.7.043702 for additional technical details and videos.

[24] D. A. Saville, Stability of electrically charged viscous cylinders, Phys. Fluids **14**, 1095 (1971).

[25] L. L. F. Agostinho, G. Tamminga, C. U. Yurteri, S. P. Brouwer, E. C. Fuchs, and J. C. M. Marijnissen, Morphology of water electrosprays in the simple-jet mode, Phys. Rev. E **86**, 066317 (2012).

[26] L. L. F. Agostinho, C. U. Yurteri, E. C. Fuchs, and J. C. M. Marijnissen, Monodisperse water microdroplets generated by electrohydrodynamic atomization in the simple-jet mode, Appl. Phys. Lett. **100**, 244105 (2012).

[27] B. Ambravaneswaran, H. J. Subramani, S. D. Phillips, and O. A. Basaran, Dripping-Jetting Transitions in a Dripping Faucet, Phys. Rev. Lett. **93**, 034501 (2004).

[28] H. González and F. J. García, The measurement of growth rates in capillary jets, J. Fluid Mech. **619**, 179 (2009).

[29] M. G. V. Bogle, J. E. Hearst, V. F. R. Jones, and L. Stoilov, Lissajous knots, J. Knot Theory Ramifications **03**, 121 (1994).

[30] A. J. Danner, H. L. Dao, and T. Tyc, The Lissajous lens: A three-dimensional absolute optical instrument without spherical symmetry, Opt. Express **23**, 5716 (2015).

[31] H. Xia, B. Yu, K. Chang, X. Zhao, and W. Deng, Shaping electrospray deposition profile by a quadrupole: From circular to elliptical patterns, J. Aerosol Sci. **154**, 105739 (2021).

[32] M. Lauricella, F. Cipolletta, G. Pontrelli, D. Pisignano, and S. Succi, Effects of orthogonal rotating electric fields on electrospinning process, Phys. Fluids **29**, 082003 (2017).